RSC Advances

PAPER

View Article Online
View Journal | View Issue

Check for updates

Cite this: *RSC Adv.*, 2020, **10**, 3122

Investigation on the role of different conductive polymers in supercapacitors based on a zinc sulfide/reduced graphene oxide/conductive polymer ternary composite electrode†

Zichen Xu, Zhiqiang Zhang, Huiling Yin, Shengxian Hou, Hongtao Lin,* Jin Zhou and Shuping Zhuo*

Conductive polymers, such as polyaniline (PANI), polypyrrole (PPy), polythiophene (PTh) and poly 3,4-ethylenedioxythiophene (PEDOT), play an important role in the application of pseudocapacitors. It is necessary to explore the effects of different conductive polymers in electrode composites. Herein, we prepare zinc sulfide/reduced graphene oxide (ZnS/RGO) by the hydrothermal method, and conductive polymers (PANI, PPy, PTh and PEDOT) doped with the same mass ratio (polymer to 70 wt%) *via in situ* polymerization on the surface of ZnS/RGO composite. For the supercapacitor application, the ZnS/RGO/PANI ternary electrode composite possesses the best capacitance performance and cycle stability out of all of the polymer-coated ZnS/RGO composites. In the three-electrode system, the discharge specific capacitance and cycle stability of ZnS/RGO/PANI are 1045.3 F g^{-1} and 160% at 1 A g^{-1} after 1000 loops. In a two-electrode symmetric system, the discharge specific capacitance and cycle stability of ZnS/RGO/PANI are 722.0 F g^{-1} and 76.1% at 1 A g^{-1} after 1000 loops, and the greatest energy and power density of the ZnS/RGO/PANI electrode are 349.7 W h kg^{-1} and 18.0 kW kg^{-1}. In addition, conductive polymers can effectively improve the voltage range of the electrode composites in 6 M KOH electrolyte for the two-electrode system. The discharge voltage ~1.6 V makes them promising electrode materials for supercapacitors.

Received 27th September 2019
Accepted 13th January 2020

DOI: 10.1039/c9ra07842h

rsc.li/rsc-advances

Open Access Article. Published on 17 January 2020. Downloaded on 5/7/2026 4:29:57 PM.
This article is licensed under a Creative Commons Attribution-NonCommercial 3.0 Unported Licence.

1. Introduction

Supercapacitors (SCs) are one of the most efficient energy storage technologies to solve the serious issues of energy shortage and environmental pollution for mankind's sustainable development.[1] A supercapacitor is composed of two electrodes, an electrolyte and separator, where the electrode material is important for the electrochemical performance of SCs.[1,2] According to the energy storage mechanism, SCs can be divided into two types, electric double-layer capacitors (EDLCs) based on electrostatic interaction between the electrode material and the electrolyte, and pseudocapacitors *via* quick and reversible faradaic redox reaction on the surface between the electrode materials and electrolyte ions.[3,4] Typically, pseudocapacitors can store more capacitance than EDLCs but the kinetics of pseudocapacitors is slower than that of EDLCs. This is because the energy storage process in pseudocapacitors occurs in the bulk of the electrode material, while for EDLCs the charge/discharge process only occurs on the surface of the electrode materials.[4–6] Therefore, a two-dimensional layered electrode material with multiple active sites can greatly improve the capacitance and reduce the dynamic effects, which is a promising electrode material for pseudocapacitors.

To obtain a promising electrode material for pseudocapacitors, metal sulfides such as MoS_2,[7] SnS_2,[8] CoS[9] and ZnS[8] have been widely concerned with their excellent electrical conductivity, multiple active sites and low-cost. Compared to the limitations of electrode materials with single substance in the application of actual conditions, composite electrode materials possess better environmental stability and low-cost in the application of SCs. Composite electrode materials can also achieve better electrochemical performance by controlling their morphology. For example, Ramachandran *et al.*[10] synthesized zinc sulfide decorated graphene (ZnS/G) nanocomposites *via* a facile solvothermal approach and its specific capacitance is up to 197.1 F g^{-1} at 5 mV s^{-1} in 6 M KOH electrolyte, which is better than the specific capacitance of ZnS as 32.8 F g^{-1} and that of graphene as 115 F g^{-1}. Graphene as a typical two-dimensional material can improve the surface area of composites and prevent metal sulfide accumulation

School of Chemistry and Chemical Engineering, Shandong University of Technology, Zibo 255000, P. R. China. E-mail: linht@sdut.edu.cn

† Electronic supplementary information (ESI) available. See DOI: 10.1039/c9ra07842h

This journal is © The Royal Society of Chemistry 2020

Open Access Article. Published on 17 January 2020. Downloaded on 5/7/2026 4:29:57 PM.
This article is licensed under a Creative Commons Attribution-NonCommercial 3.0 Unported Licence.

because of the effect of its conjugated π bonds.[11,12] Although graphene/metal sulfides composites have excellent electroconductibility and stable capacity performance, but poor capacitance and energy performance limit its application in pseudocapacitors.[13] Therefore, doping a high capacitance material for pseudocapacitors, such as conductive polymers, may be an effective method *t* for improving the electrochemical performance of pseudocapacitors.

Conductive polymers (CPs) such as polyaniline (PANI), polypyrrole (PPy), polythiophene (PTh) and poly 3,4-ethylenedioxythiophene (PEDOT) are regarded as promising pseudocapacitive materials because of their large specific capacitance and the characterization of many active sites.[14] However, pure CPs are easier to accumulate into blocks and the contact areas between polymers and electrolyte are decreased, which reduces the electrochemical properties. Therefore, this composite with a lone pair of electrons and two-dimensional planar structure, such as graphene/metal sulfides, can effectively prevent the accumulation of CPs and improve the cycle stability of CPs.[15–17] For example, Li *et al.*[18] successfully synthesized MoS_2/RGO@PANI electrode composite through a two-stage synthetic method, and the specific capacitance and cycle stability after 3000 loops of MoS_2/RGO@PANI at 1 A g^{-1} were 1224 F g^{-1} and 82.5%, which were better than those of pure PANI as 774 F g^{-1} and 70.2%. Tang *et al.*[19] has developed a scalable solution-based approach to controllable growth of PPy ultrathin films on two-dimensional MoS_2 monolayers and the specific capacitance and cycle stability of MoS_2/PPy (695 F g^{-1}, 85% at 1 A g^{-1} after 4000 cycles) are far more than those of PPy (200 F g^{-1}, 60% at 1 A g^{-1} after 4000 cycles). The results indicate that the synergistic effect among polymer, metal sulfide and graphene can effectively improve electrochemical performance of electrode materials.[18,19] But various CPs have different effect on the electrode composites, which may be ascribed to their discrepant conductive and growth mechanism. So, it is necessary to study how various CPs improve electrochemical performance of electrode composites.

Herein, we chose to prepare ZnS/reduced graphene oxide (ZnS/RGO) by hydrothermal method, and CPs (PANI, PPy, PTh and PEDOT) doped with the same mass ratio (polymer to 70 wt%) *via in situ* polymerization on the surface of ZnS/RGO composite. CPs can effectively improve capacitance performance of electrode composites, and it also extended the voltage range in two-electrode system. In 6 M KOH electrolyte solution, the voltage range of various polymer-coated ZnS/RGO electrode with two-electrode system are up to 0–1.6 V, which is better than that (−0.2–0.6 V) in three-electrode system and improve energy and power density of electrode composites. For the application of SCs, ZnS/RGO/PANI possesses the best electrochemical properties respectively in two and three electrode system, and it is a promising electrode material of pseudocapacitors. These findings may be useful for developing effective and stable electrode materials for energy storage device.

2. Experimental section

2.1 Preparation of ZnS/RGO hybrid materials

Graphene oxide (GO) was produced using the modified Hummers' method from the graphite powder.[20] ZnS/RGO was first prepared in a typical process. 1.22 g of $Zn(NO_3)_2 \cdot 6H_2O$ and 100 mg of GO were added into 50 mL deionized water, and then 611 mg of thiocarbamide (CH_4N_2S) were added which provides sulfur sources and acts as a reducing agent. After the mixture was stirred for 1 h, brown suspension was obtained. The mixture was then transferred into a 100 mL Teflon stainless steel autoclave, sealed, and heated at 180 °C for 12 h in an oven. After cooled to room temperature under natural conditions, the precipitations was collected with centrifugation and washed several times by ethanol and deionized water, and then dried under vacuum freeze-drying for 24 h. The binary composite material ZnS/RGO was obtained finally.

2.2 Preparation of ZnS/RGO/CPs ternary composites

In our previous work, we found when 70 wt% PPy to ZnS/RGO/PPy, the ZnS/RGO/PPy ternary composite has the best electrochemical performance and morphology.[21] Therefore, we designed that PANI, PPy, PTh and PEDOT were separately grown on the surface of the obtained ZnS/RGO composite *via in situ* polymerization, and the mass ratio of the polymer was 70%. The preparation method is divided into four parts as follows:

I. The preparation of ZnS/RGO/PANI. 233.3 mg of aniline (An) was added to 50 mL HCl (pH = 3) suspension with 100 mg of ZnS/RGO composite. Then, 350 mg of ammonium persulfate ($(NH_4)_2S_2O_8$, APS) was added in batches to the above suspension and it was stirred in an ice bath (~1 °C) for 24 h.

II. The preparation of ZnS/RGO/PPy. 154 μL of pyrrole (Py) and 0.911 g cetyltrimethylammonium bromide (CTAB) were added to 50 mL of HCl (0.3 mol L^{-1}) suspension with 100 mg of ZnS/RGO composite. Then, 1.81 g ferric chloride ($FeCl_3$) was added in batches to the above suspension and it was stirred in an ice bath (~1 °C) for 24 h.

III. The preparation of ZnS/RGO/PTh. 100 mg of ZnS/RGO was ultrasonically dispersed in 20 mL of nitromethane (CH_3NO_2), then 1.0 g of $FeCl_3$ was added and stirred for 30 min. The above solution was added dropwise to 10 mL of *n*-hexane solvent containing 220 μL of thiophene (Th) and continuously stirred at room temperature for 24 h.

IV. The preparation of ZnS/RGO/PEDOT. 100 mg ZnS/RGO was ultrasonically dispersed in 50 mL deionized water and obtained suspension. 10 mL of acetonitrile solution dissolved in 174 μL of 3, 4-ethylenedioxythiophene (EDOT) was added dropwise to the above suspension and stirred for 1 h. Then, 458 mg APS was added to the above mixed solution and stirred in an ice bath (~1 °C) for 24 h.

All of the obtained precipitates were washed by deionized water and ethanol, and freeze-drying for 24 h. Finally, we successfully synthesized four kinds of ternary composite, ZnS/RGO/PANI, ZnS/RGO/PPy, ZnS/RGO/PTh and ZnS/RGO/PEDOT. The synthesis steps was shown in Scheme 1.

Open Access Article. Published on 17 January 2020. Downloaded on 5/7/2026 4:29:57 PM.
This article is licensed under a Creative Commons Attribution-NonCommercial 3.0 Unported Licence.

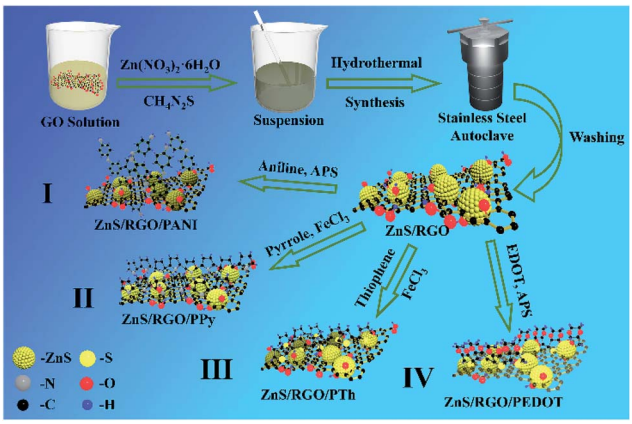

Scheme 1 The synthetic process of ZnS/RGO/CPs ternary composites.

2.3 Characterization

X-ray diffraction (XRD) measurements were conducted by using a Bruker D8 Advance diffraction (Bruker Corporation, Karlsruhe Germany) with Cu Kα radiation. The surface chemical properties were determined by X-ray photoelectron spectrometer (XPS; Escalab 250, Thermo Fisher Scientific, Waltham, Massachusetts). The microscopic morphology of the products were observed with a scanning electron microscopy (SEM; Sirion 200, FEI Company, Amsterdam, The Netherlands) and high-revolution transmission electron microscopy (HRTEM; Tecnai G2TF20 S-TWIN, FEI Company) at a working voltage of 200 kV. The nitrogen sorption isotherm was achieved at 77.3 K on a Micromeritics ASAP2020HD88 gas sorptometer (Micromeritics, U.S.A.). The molecular structure and composition of the products were analyzed by KBr method on a Fourier Transform Infrared (FT-IR) spectrometer (Nicolet 5700, Thermo Company, America).

2.4 Electrochemical measurements for supercapacitor

Cyclic voltammetry (CV), galvanostatic charge–discharge (GCD) and electrochemical impedance spectroscopy (EIS) were measured by a CHI660C (Chenhua Instruments Co. Ltd. Shanghai, China) electrochemical workstation. Working electrode was prepared by mixing electroactive materials and polyterafluoro-ethylene (PTFE) in a mass ratio of 95 : 5 and was loaded on low-capacitance nickel foam through mechanical pressure plates. The effective area of working electrode was 1.5 × 1.0 cm. In three-electrode system, a platinum electrode was counter electrode and a mercury/mercury oxide electrode was reference electrode in 6 M KOH electrolyte solution. In two-electrode system, the preparation of positive and negative was consistent with that of the above working electrode and 6 M KOH as electrolyte.

3. Results and discussion

Fig. 1a displays the XRD patterns of theses ternary composites based on CPs and ZnS/RGO. The diffraction peaks at 28.6°, 47.5° and 56.4° are corresponding to the planes of (111), (220) and (311) respectively, which is consistent with the characteristic peaks of ZnS (JCPDS No. 65-9585). The lattice spacing of ZnS nanoparticles is 0.32 nm, which is calculated by the Debye–Scherrer formula based on the full width at half-maximum of the (111) diffraction peak.[22] No peaks at around 10° displays that graphene oxide has been reduced and the wide peaks at about 20–30° indicates the presence of disordered polymers.[23,24] FT-IR spectrum, as an effective and sensitive tool to give direct evidence of polymer formation, is shown in Fig. 1b, which displays distinct contrast between the ternary composites and pristine polymers. The band at 437 cm^{-1} arises from the E_2 mode of hexagonal ZnS,[25] which exists in all the FT-IR spectra of the polymer-coated ZnS/RGO ternary composite. The characteristic bands of different polymers are observed in the FT-IR spectra of ternary composites. ZnS/RGO/PEDOT demonstrates C–S and C–O–R stretching vibration of PEDOT at around 917 and 1210 cm^{-1}.[26,27] Besides the single spectrum of PTh, ZnS/RGO/PTh presents not only C–S vibration, but also intense C=C stretching vibration at 1557 cm^{-1}, which indicates the presence of graphene.[28] ZnS/RGO/PPy shows the C–N and pyrrole ring stretching vibration of PPy at around 1190 and 1464 cm^{-1}.[29,30] ZnS/RGO/PANI not only exhibits the quinoid ring and benzenoid ring stretching vibration of PANI at 1496 and 1580 cm^{-1}, but the bands of C–N stretching vibration located between 1200 and 1400 cm^{-1}.[31,32] These results verify that the polymers, PEDOT, PTh, PPy and PANI, are successful synthesized on the surface of ZnS/RGO composite.

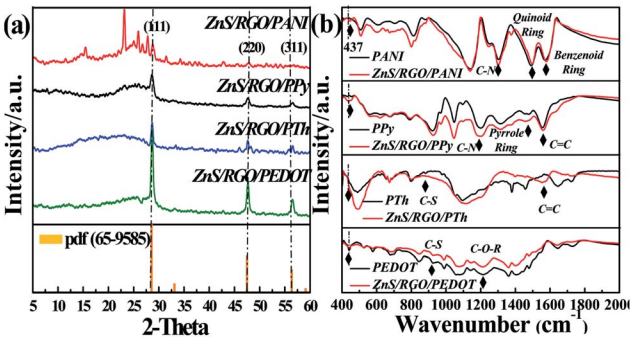

Fig. 1 The XRD patterns (a) and FT-IR spectra (b) of ZnS/RGO/PANI, ZnS/RGO/PPy, ZnS/RGO/PTh and ZnS/RGO/PEDOT.

Polymer-coated ZnS/RGO ternary composites are explored as an electrode material in 6 M KOH electrolyte solution for three-electrode system, where nickel foam as current collector. The electrochemical characterization of polymer-coated ZnS/RGO ternary electrode materials is targeted in Fig. 2. Besides a single CV curve of nickel foam, the redox peaks intensity of polymer-coated ZnS/RGO electrode materials are enhanced as shown in Fig. 2a. The values of oxidation and reduction peak of ZnS/RGO/PANI are 0.36 and 0.26 V respectively, which is lower than those of the ZnS/RGO/PPy and ZnS/RGO/PTh (0.38 and 0.28 V). ZnS/RGO/PEDOT has a similar value of redox peak to nickel foam (0.39 and 0.29 V). ZnS/RGO/PANI has the largest integrate area in CV curves and GCD profiles as shown in Fig. 2a

 This journal is © The Royal Society of Chemistry 2020

Open Access Article. Published on 17 January 2020. Downloaded on 5/7/2026 4:29:57 PM.
This article is licensed under a Creative Commons Attribution-NonCommercial 3.0 Unported Licence.

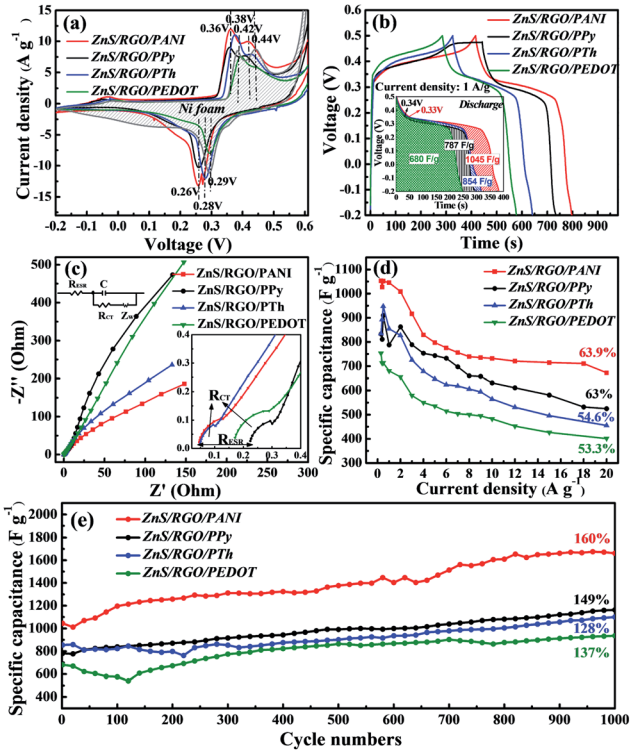

Fig. 2 In three-electrode system,(a) CV curves at 10 mV s^{-1}, (b) GCD profiles and discharge curves (illustration) at 1 A g^{-1}, (c) high frequency (illustration) and low frequency Nyquist plots at frequency range from 100 kHz to 0.01 Hz, (d) capacitance performance at the range of current density from 0.3 to 20 A g^{-1} and (e) cycle performance of ZnS/RGO/PANI, ZnS/RGO/PPy, ZnS/RGO/PTh and ZnS/RGO/PEDOT.

and b, which indicates that it has excellent specific capacitance property. The specific capacitance of ZnS/RGO/PANI at 1 A g^{-1} is up to 1045 F g^{-1}, which is larger than that of the ZnS/RGO/PTh (854 F g^{-1}), ZnS/RGO/PPy (787 F g^{-1}) and ZnS/RGO/PEDOT (680 F g^{-1}). Meanwhile, the specific capacitance of ZnS/RGO/PANI (1045 F g^{-1} at 1 A g^{-1}) is also better than other composites reported, such as GO/PANI (425 F g^{-1} at 0.2 A g^{-1}),[33] ZnS/G-60 (191.7 F g^{-1} at 5 mV s^{-1}),[10] PANI/Zn^{2+} film (738 F g^{-1} at 5 mA cm^{-2}),[34] rGO/Fe_3O_4/PANI (283.4 F g^{-1} at 1 A g^{-1})[35] and SnS_2/NRGO/PANI (1021.7 F g^{-1} at 1 A g^{-1}).[31] The specific capacitance (C_S) of faradaic pseudocapacitance for three-electrode system can be calculated based on the following equation:[36]

$$C_S = \left(2i_m \int V\mathrm{d}t\right) \Big/ \left(V^2|_{V_i}^{V_f}\right) \ (\mathrm{F\ g^{-1}}) \qquad (1)$$

where i_m (A g^{-1}) is the current density, I (A) is the discharge current and m (g) is the active mass of the electrode. $\int V\mathrm{d}t$ is the integral current area, where V is the potential with initial and final values of V_i and V_f, respectively.

We speculate that the difference in the electrochemical properties for the polymer-coated ZnS/RGO electrode materials are attributed to the different conductive mechanism for the polymers. PANI depolarizes a positive charge on a nitrogen atom into a large conjugated π bond *via* a redox reaction, thereby obtaining high conductivity.[37,38] However, PPy and PTh have similar electrical conduction mechanisms, both are transferred by conjugated π electrons.[39,40] In PEDOT, the epoxy ring provides the electron-donating group with improved conductivity but greatly increases its steric hindrance.[41,42] To confirm this speculation, we test the EIS plots of the polymer-coated ZnS/RGO electrode materials as shown in Fig. 2c. In the high and intermediated frequencies region, the semicircular portion reflects charge-transfer resistance (R_{CT}) arranged in order as ZnS/RGO/PTh (0.17 Ω) < ZnS/RGO/PPy (0.18 Ω) < ZnS/RGO/PANI (0.21 Ω) < ZnS/RGO/PEDOT (0.27 Ω). The process of redox reaction and the effect of steric hindrance result in the larger R_{CT} of ZnS/RGO/PANI and ZnS/RGO/PEDOT, respectively.[42,43] In the low frequency region, the line with a low slope predicts that it has significant faradaic pseudocapacitance performance. ZnS/RGO/PANI also possesses the best conductivity as shown in Table S1† and the values of ionic conductivity (σ) are putted in order as ZnS/RGO (0.61×10^{-3} S m^{-1}) < ZnS/RGO/PEDOT (0.74×10^{-3} S m^{-1}) < ZnS/RGO/PPy (0.81×10^{-3} S m^{-1}) < ZnS/RGO/PTh (1.46×10^{-3} S m^{-1}) < ZnS/RGO/PANI (1.77×10^{-3} S m^{-1}). Not only that, ZnS/RGO/PANI also has excellent capacitance retention as 63.9% at different current density from 0.3 to 20 A g^{-1} in Fig. 2d, which is higher than that of ZnS/RGO/PPy (63%), ZnS/RGO/PTh (54.6%) and ZnS/RGO/PEDOT (53.3%). Simultaneously, ZnS/RGO/PANI possesses the largest discharge specific capacitance at various current densities and it still remains 672.6 F g^{-1} when the current density reaches to 20 A g^{-1}. As the cycle numbers increase, the discharge specific capacitance of all polymer-coated ZnS/RGO electrode materials are increased as shown in Fig. 2e. ZnS/RGO/PANI has the largest growth rate as 160% and its discharge specific capacitance is up to 1662 F g^{-1} at 1 A g^{-1} after 1000 cycles, which is better than those of composites reported, such as GO/PANI (83% after 500 cycles),[33] ZnS/G-60 (94.1% after 1000 cycles),[10] PANI/Zn^{2+} film (65.4% after 500 cycles),[34] rGO/Fe_3O_4/PANI (78% after 1000 cycles)[35] and SnS_2/NRGO/PANI (82% after 1000 cycles).[31] In addition, the electrochemical characterizations of ZnS/RGO electrode material are targeted in Fig. S1c–g,† which display the low capacitance retention as 44%, poor cycle stability as 88% and low specific capacitance as 425.4 F g^{-1}. And the electrochemical performance of four pure CPs is also displayed in Fig. S2a–d,† which introduces that PEDOT has the best capacitance performance (the highest value is 718.2 F g^{-1} at 0.3 A g^{-1}) than the others (PANI, 642.6 F g^{-1} at 0.3 A g^{-1}; PPy, 586.2 F g^{-1} at 0.3 A g^{-1}; PTh, 697.1 F g^{-1} at 0.3 A g^{-1}) and PTh has the same trend as PEDOT in the change of specific capacitance with different current density. Meanwhile, PANI and PPy have the smaller R_{CT} than the both PTh and PEDOT, it indirectly proves that PANI and PPy have better electronic conductivity than those of PTh and PEDOT, which is mainly reflected in the capacitance retention rate (PANI (64.0%) > PPy (56.4%) > PEDOT (54.3%) > PTh (51.6%)). However, the electrochemical properties of the above polymer-coated ZnS/RGO electrode materials are better than those of ZnS/RGO and four pure CPs, which indicates that the interaction between CPs and ZnS/RGO in composites can effectively improve the electrochemical performance of ZnS/RGO and CPs electrode.

Open Access Article. Published on 17 January 2020. Downloaded on 5/7/2026 4:29:57 PM.
This article is licensed under a Creative Commons Attribution-NonCommercial 3.0 Unported Licence.

According to above studied results, we have found that ZnS/RGO/PANI composite has the best capacitance performance and cycle stability in polymer-coated ZnS/RGO composites. We further explore what the effects of various ingredients on the electrochemical of ZnS/RGO/PANI composite. So we tested the electrochemical properties of ZnS/RGO/PANI, ZnS/RGO, PANI and RGO/PANI (the mass ratio of PANI is 70% as same as that of ZnS/RGO/PANI) with 6 M KOH electrolyte in three-electrode system as shown in Fig. S3.† As shown in Fig. S3a andb,† ZnS/RGO/PANI possesses the best capacitance performance and smart pseudocapacitor behavior, and the specific capacitance at 1 A g^{-1} can be calculated by eqn (1) as 1045.3 F g^{-1} (ZnS/RGO/PANI) > 703.9 F g^{-1} (RGO/PANI) > 568.7 F g^{-1} (PANI) > 425.4 F g^{-1} (ZnS/RGO). Meanwhile the R_{CT} of different composites is stored as ZnS/RGO/PANI < ZnS/RGO < RGO/PANI < PANI, and the capacitance retention at current density from 0.3 to 20 A g^{-1} ordered as 63.9% (ZnS/RGO/PANI) > 63.8% (PANI) > 54.8% (RGO/PANI) > 44.0% (ZnS/RGO) as shown in Fig. S3c and d.† To sum up, we speculate that ZnS plays an important role in promoting the dispersion and polymerization of PANI in ZnS/RGO/PANI composite system. Because, PANI is easy to stack, which causes its poor capacitance performance, but when it compounded with graphene can effectively improve its dispersion and capacitance performance. However, when PANI grows on the surface of ZnS/RGO, its specific capacitance and conductivity will be further improved. It is indicated that ZnS particles can strengthen the connection between PANI and graphene, which is beneficial to the transfer of electrons in ZnS/RGO/PANI ternary composite.

As we all know, the electrochemical performances of the electrode materials are inextricably related to their morphologies. By SEM and TEM images, we can clearly observe the successful deposition of PANI, PPy, PTh and PEDOT on the surface of layered ZnS/RGO. As shown in the SEM and TEM images of ZnS/RGO composite (Fig. S1a and b†), ZnS spherical particles are distributed on the tissue-like RGO layer and its lattice spacing is 0.32 nm. Compared to the morphology of ZnS/RGO, all the polymer-coated ZnS/RGO materials remain the spherical shape of ZnS and the layered structure of graphene as shown in Fig. 3a–d. Meanwhile, the surfaces become more fluffy and multi-layered for all the polymer-coated ZnS/RGO composites. This fluffy multi-layered morphology causes the electrolyte gradually penetrate from the outside to the interior of electrode materials and activate more active sites as cycle numbers increases, which further promotes their capacitance performance. As targeted in Fig. 3a–d, the EDS images of various polymer-coated ZnS/RGO composites display distribution and percentage of the elements: ZnS/RGO/PANI (C: 46.14%, N: 42.9%, S: 5.07%, Zn: 5.62%), ZnS/RGO/PPy (C: 68.1%, N: 21.9%, S: 5.05%, Zn: 4.95%), ZnS/RGO/PTh (C: 47.54%, O: 17.61%, S: 18.2%, Zn: 16.65%) and ZnS/RGO/PEDOT (C: 14.8%, O: 44.1%, S: 28.87%, Zn: 12.24%). N and S elements doped in the composites provide more active sites, which makes them possess better capacitance performance.[44,45] ZnS/RGO/PANI possesses the largest percentage of N and S elements, which explains the reason for the largest specific capacitance of ZnS/RGO/PANI (Fig. 2d). As shown in Fig. 3e–h, the TEM images further exhibit the morphologies of polymer-coated ZnS/RGO composites. The ZnS lattice spacing for all the composites is 0.32 nm, which is consistent with the plane (111) calculated by XRD in Fig. 1a. Various polymers have different morphologies, such as PANI in the shape of raspberry, PPy in the form of nanofibrous, PTh and PEDOT in the form of membrane structure, respectively. Meanwhile, the average thickness of different polymers on the surface of ZnS spherical particles are almost the same for the polymer-coated ZnS/RGO composites as seen in the HRTEM images (Fig. 3e–h). The specific surface areas are achieved from nitrogen sorption isotherms on the basis of Brunauer–Emmett–Teller (BET) theory (Fig. S4a–d†), and the order as follows: ZnS/RGO/PEDOT (18.18 m^2 g^{-1}) < ZnS/RGO/PTh (32.53 m^2 g^{-1}) < ZnS/RGO/PPy (40.60 m^2 g^{-1}) < ZnS/RGO/PANI (61.90 m^2 g^{-1}). Their pore distributions are mainly dominated by micropores and macropores, and the average pore size distributions are 10.63 nm (ZnS/RGO/PANI), 15.60 nm (ZnS/RGO/PPy), 16.65 nm (ZnS/RGO/PTh) and 13.63 nm (ZnS/RGO/PEDOT).

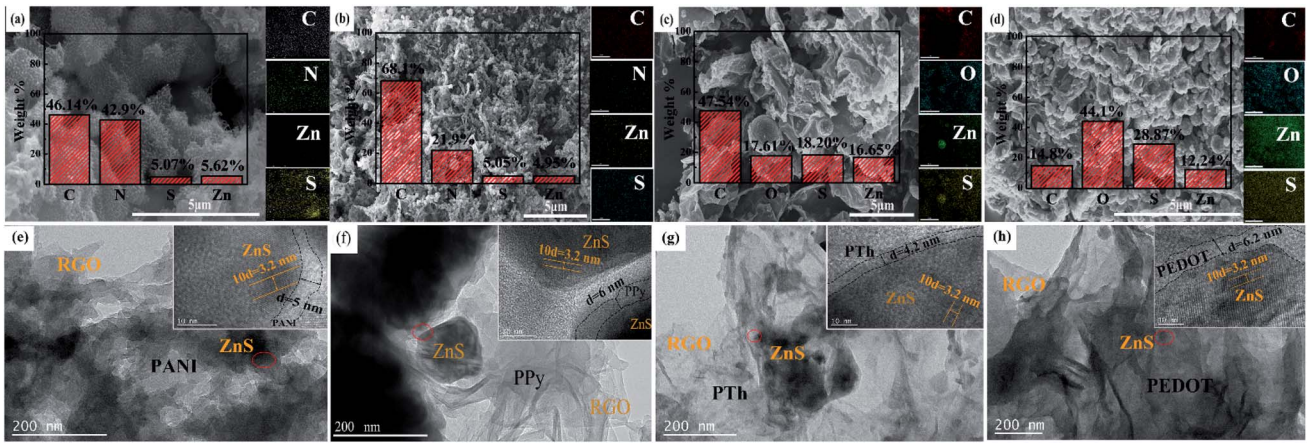

Fig. 3 The SEM and EDS images of (a) ZnS/RGO/PANI, (b) ZnS/RGO/PPy, (c) ZnS/RGO/PTh and (d) ZnS/RGO/PEDOT, and the TEM images of (e) ZnS/RGO/PANI, (f) ZnS/RGO/PPy, (g) ZnS/RGO/PTh and (h) ZnS/RGO/PEDOT.

 This journal is © The Royal Society of Chemistry 2020

Open Access Article. Published on 17 January 2020. Downloaded on 5/7/2026 4:29:57 PM.
This article is licensed under a Creative Commons Attribution-NonCommercial 3.0 Unported Licence.

Further structural properties and composition of polymer-coated ZnS/RGO composites are obtained by XPS analysis and the spectra are displayed in Fig. 4. According to the C 1s spectrum as shown in Fig. 4a, the C–N characteristic peaks of PANI and PPy at 285.0 (ZnS/RGO/PANI) and 285.2 eV (ZnS/RGO/PPy), which are corresponding to 1298.9 cm^{-1} and 1190 cm^{-1} respectively in FT-IR spectra (Fig. 1b). Meanwhile, the C–S characteristic peaks of PTh and PEDOT at 288.7 (ZnS/RGO/PTh) and 288.9 eV (ZnS/RGO/PEDOT), which are corresponding to 917 cm^{-1} in FT-IR spectra. As targeted in Fig. 4b, the N 1s spectrums of ZnS/RGO/PANI and ZnS/RGO/PPy can be categorized into four peaks as pyridinic N, C–N, pyrrolic N and Zn–N. The binding energy of N 1s for ZnS/RGO/PPy is greater than that of ZnS/RGO/PANI, which indicates that the nitrogen atoms on ZnS/RGO/PANI are more reactive. As shown in Fig. 4c, the O 1s spectrums of ZnS/RGO/PANI, ZnS/RGO/PPy and ZnS/RGO/PTh are categorized into three peaks as O–C, O=C and ROSR, which are corresponding to the bonding form of GO. But ZnS/RGO/PEDOT composite possesses the C–O–R peak at 534.0 eV, which is corresponding to the characteristic peak of PEDOT at 1210 cm^{-1} in FT-IR. In addition, the atomic percentage of various elements of these ternary composites are listed according to the XPS test in Table S2.† ZnS/RGO/PANI composite possesses the largest total percentage of N and S as 18%, which is consistent with the result in EDS graphic (Fig. 2a–d).

To further explore the application of these polymer-coated ZnS/RGO composites, we studied their electrochemical performance in a symmetric two-electrode system with 6 M KOH as electrolyte as shown in Fig. 5. As shown in Fig. 5a and b, the redox peaks in CV curves at 0.80 and 1.56 V are consistent with the voltage platform in GCD profiles and D-ZnS/RGO/PANI (double ZnS/RGO/PANI electrode) possesses the largest integrate area. The potential window of these electrode materials is extended to 1.6 V in two-electrode system, because the inherent high voltage range of the polymer improves the energy of these electrode materials. Meanwhile, electrode composites in symmetrical two-electrode system are more easily activated to reach higher potentials than those in three-electrode system, because in three-electrode system the reference electrode can precisely adjust the potential of work electrode.[46] In addition, extended potential window is also related to the electrolyte especially pH and concentration, which affects the diffusion of ions in the electrolyte solution.[47] In this work, we use 30 mL of 6 M KOH as electrolyte, and its pH is around 13. In the GCD profiles, the discharge specific capacitance (C_S) of these ternary composites in two-electrode system can be calculated by follow equation based on eqn (1):

$$C_S = 2I\left(2\int V\mathrm{d}t\right)\Big/ m\left(V^2\Big|_{V_i}^{V_f}\right) \quad (\mathrm{F\ g^{-1}}) \qquad (2)$$

where I (A) is the discharge current and m (g) is the active mass of the single electrode. $\int V\mathrm{d}t$, V_i and V_f are the same function in eqn (1).

According to eqn (2), the discharge specific capacitance at the current density of 1A g^{-1} are 722.0 (D-ZnS/RGO/PANI), 613.8 (D-ZnS/RGO/PPy), 564.3 (D-ZnS/RGO/PTh) and 653.4 F g^{-1} (D-ZnS/RGO/PEDOT), respectively. D-ZnS/RGO/PANI has the

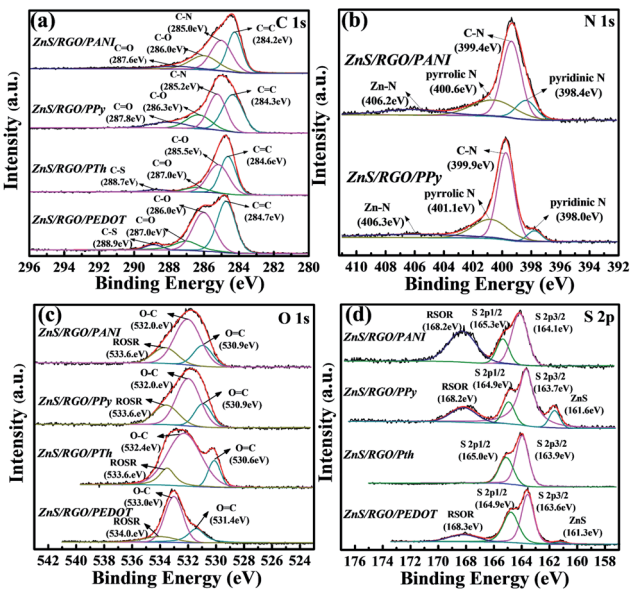

Fig. 4 Deconvoluted XPS spectra: the high-resolution spectra (a) C 1s, (b) N 1s, (c) O 1s and (d) S 2p of ZnS/RGO/PANI, ZnS/RGO/PPy, ZnS/RGO/PTh and ZnS/RGO/PEDOT.

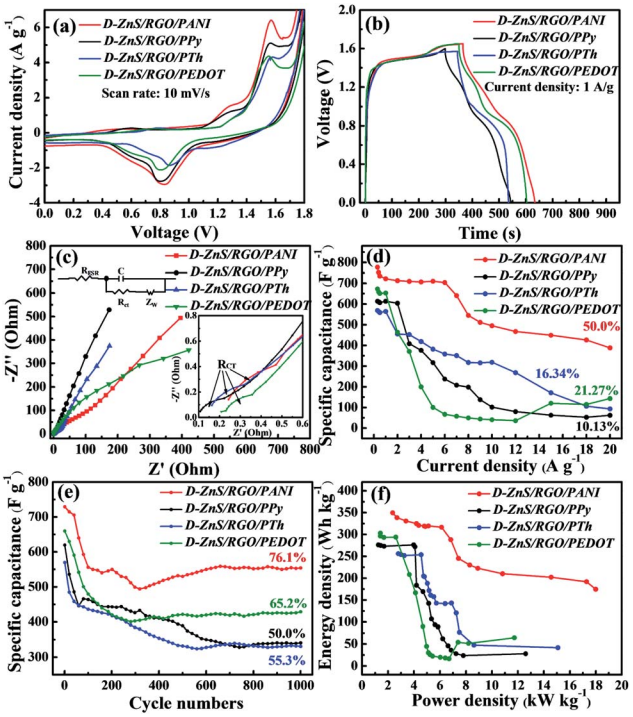

Fig. 5 Electrochemical characterization of symmetric two-electrode system of ZnS/RGO/PANI, ZnS/RGO/PPy, ZnS/RGO/PTh and ZnS/RGO/PEDOT: (a) CV curves at scan rate of 10 mV s^{-1}, (b) GCD profiles at current density of 1 A g^{-1}, (c) EIS plots at the range of low frequency and high frequency (illustration), (d) the properties of discharge specific capacitance at different current density, (e) the cycle performance at 1 A g^{-1} and (f) Ragone plots of symmetric supercapacitors.

Open Access Article. Published on 17 January 2020. Downloaded on 5/7/2026 4:29:57 PM.
This article is licensed under a Creative Commons Attribution-NonCommercial 3.0 Unported Licence.

largest discharge specific capacitance, which is ascribed to the maximum percentage of N and S elements on the surface of ZnS/RGO/PANI (Fig. 3a and Table S2†). As shown in Fig. 5c, D-ZnS/RGO/PANI also has the smallest slope of a line in the range of low frequency because of its significant redox reaction on the surface. In the range of high frequency, R_{CT} are arrayed as D-ZnS/RGO/PPy (0.30 Ω) < D-ZnS/RGO/PTh (0.37 Ω) < D-ZnS/RGO/PEDOT (0.56 Ω) < D-ZnS/RGO/PANI (0.93 Ω), which are around twice than the R_{CT} in three-electrode system as shown in Fig. 2c. The discharge specific capacitance of various composites at different current density are calculated by eqn (2) as shown in Fig. 5d. The initial values of these composites at the current density of 0.3 A g^{-1} are 777.2 (D-ZnS/RGO/PANI), 613.8 (D-ZnS/RGO/PPy), 569.3 (D-ZnS/RGO/PTh) and 673.2 F g^{-1} (D-ZnS/RGO/PEDOT), and their capacitance retention are 50.0% (D-ZnS/RGO/PANI), 10.13% (D-ZnS/RGO/PPy), 16.34% (D-ZnS/RGO/PTh) and 21.27% (D-ZnS/RGO/PEDOT) respectively when the current density is up to 20 A g^{-1}. D-ZnS/RGO/PANI possesses the best capacitance performance because of its unique conductive mechanism from the constant conversion of oxidation and reduction states. This result also displays the difference between symmetric two-electrode system and three-electrode system. D-ZnS/RGO/PANI shows the best capacitance performance, which is consistent with the tests of three-electrode system in Fig. 2d. Meanwhile, D-ZnS/RGO/PANI also possesses the highest cycle stability as 76.1% in the above composites at the current density of 1 A g^{-1} as shown in Fig. 5e and its specific capacitance is slightly improved after 300 cycles, which is because of the raspberry-like PANI structure (Fig. 3a) and microporous structure (Fig. S4a†) favorable for electrolyte penetration. And the specific capacitance of D-ZnS/RGO/PEDOT is also slightly improved after 300 cycles. Because the surface of both ZnS/RGO/PANI and ZnS/RGO/PEDOT has dense polymer coatings, which leads their specific capacitance to decreasing in the first 300 cycles. As the cycles increasing, the surface of ZnS/RGO/PANI and ZnS/RGO/PEDOT has been fully activated to accommodate more ions, thereby increasing the value of their specific capacitance, and finally their specific capacitance reaches stability. In addition, D-ZnS/RGO/PEDOT (65.2%) has better cycle stability than D-ZnS/RGO/PTh (55.3%) and D-ZnS/RGO/PPy (50.0%), because membrane PEDOT structure (Fig. 3d and h) has better structural stability.

Energy density (E) and power density (P) as important parameters to measure the performance of symmetric supercapacitors can be calculated by follow equations:

$$E = (1/7.2) \times \Delta V^2 \times C_S \text{ (W h kg}^{-1}\text{)} \quad (3)$$

$$P = 3600E/\Delta t \text{ (W kg}^{-1}\text{)} \quad (4)$$

where C_S (F g^{-1}) is discharge specific capacitance, Δt (s) is the discharge time and ΔV (V) represents the potential drop during the discharge process.

As shown in Fig. 5f, D-ZnS/RGO/PANI exhibits the excellent values of energy and power density in the range of 0.3–20 A g^{-1}, and the greatest energy and power density are calculated using eqn (3) and (4) to 349.7 W h kg^{-1} and 18.0 kW kg^{-1}, respectively. These results are better than the reported symmetric supercapacitors based on PANI, such as MoS_2/RGO/PANI (22.3 W h kg^{-1} and 5.1 kW kg^{-1}),[14] rGO/Fe_3O_4/PANI (47.7 W h kg^{-1} and 550 W kg^{-1}),[35] SnS_2/NRGO/PANI (69.5 W h kg^{-1} and 575.5 W kg^{-1})[31] and ternary nitrogen-doped graphene/nickel ferrite/polyaniline (92.7 W h kg^{-1} and 110.8 W kg^{-1}).[48]

4. Conclusions

In summary, conductive polymers such as PANI, PPy, PTh and PEDOT have been successfully synthesized on the surface of ZnS/RGO layered composites *via in situ* polymerization. We have obtained four identical mass ratios of polymer-coated ZnS/RGO ternary composites. Thus, the four polymers effectively improve cycle stability and discharge specific capacitance of ZnS/RGO electrode for supercapacitors, while the ZnS/RGO/PANI composite possesses the best performances. Meanwhile, we have also assembled symmetric two-electrode supercapacitors by using these composites. It is found that all of them immensely extend the potential window of electrodes in 6 M KOH electrolyte to achieve more excellent energy and power density. Double ZnS/RGO/PANI (D-ZnS/RGO/PANI) electrode is the best of them. The discharge specific capacitance of ZnS/RGO/PANI is 1045.3 and 722.0 F g^{-1} at 1 A g^{-1} in a three-electrode and two-electrode system, respectively. In a two-electrode symmetric system, the greatest energy and power density of ZnS/RGO/PANI electrode are 349.7 W h kg^{-1} and 18.0 kW kg^{-1}. In addition, the cycle stability of ZnS/RGO/PANI electrode is 160% and 76.1% in a three-electrode and two-electrode system, respectively. It is ascribed to raspberry-like fluffy structure and N, S multiple active sites of ZnS/RGO/PANI electrode promote electrolyte penetration and activate more active sites during cycling. The superior performances of the ZnS/RGO/PANI electrode will be applied to high energy power supercapacitors.

Conflicts of interest

There are no conflicts to declare.

Acknowledgements

This work was supported by the National Natural Science Foundation of China (No. 21403130, 21403129, 21576158, 21576159), the Natural Science Foundation of Shandong Province (ZR2014BQ028, 2015ZRB01765).

Notes and references

1 P. Simon and Y. Gogotsi, *Nat. Mater.*, 2008, **7**, 845.
2 R. Kötz and M. Carlen, *Electrochim. Acta*, 2000, **45**, 2483–2498.
3 C. Largeot, C. Portet, J. Chmiola, P.-L. Taberna, Y. Gogotsi and P. Simon, *J. Am. Chem. Soc.*, 2008, **130**, 2730–2731.
4 G. A. Snook, P. Kao and A. S. Best, *J. Power Sources*, 2011, **196**, 1–12.

 This journal is © The Royal Society of Chemistry 2020

Open Access Article. Published on 17 January 2020. Downloaded on 5/7/2026 4:29:57 PM.
This article is licensed under a Creative Commons Attribution-NonCommercial 3.0 Unported Licence.

5 D. Ni, Y. Chen, X. Yang, C. Liu and K. Cai, *J. Alloys Compd.*, 2018, **737**, 623–629.
6 Y. Chen, D. Ni, X. Yang, C. Liu, J. Yin and K. Cai, *Electrochim. Acta*, 2018, **278**, 114–123.
7 X. Geng, Y. Zhang, Y. Han, J. Li, L. Yang, M. Benamara, L. Chen and H. Zhu, *Nano Lett.*, 2017, **17**, 1825–1832.
8 N. Parveen, S. A. Ansari, H. R. Alamri, M. O. Ansari, Z. Khan and M. H. Cho, *ACS Omega*, 2018, **3**, 1581–1588.
9 Z. Yang, C.-Y. Chen and H.-T. Chang, *J. Power Sources*, 2011, **196**, 7874–7877.
10 R. Ramachandran, M. Saranya, P. Kollu, B. P. C. Raghupathy, S. K. Jeong and A. N. Grace, *Electrochim. Acta*, 2015, **178**, 647–657.
11 J. J. Yoo, K. Balakrishnan, J. Huang, V. Meunier, B. G. Sumpter, A. Srivastava, M. Conway, A. L. Mohana Reddy, J. Yu, R. Vajtai and P. M. Ajayan, *Nano Lett.*, 2011, **11**, 1423–1427.
12 Y. Wang, Z. Shi, Y. Huang, Y. Ma, C. Wang, M. Chen and Y. Chen, *J. Phys. Chem. C*, 2009, **113**, 13103–13107.
13 N. Mahmood, C. Zhang, H. Yin and Y. Hou, *J. Mater. Chem. A*, 2014, **2**, 15–32.
14 Q. Meng, K. Cai, Y. Chen and L. Chen, *Nano Energy*, 2017, **36**, 268–285.
15 L. Tong, M. Gao, C. Jiang and K. Cai, *J. Mater. Chem. A*, 2019, **7**, 10751–10760.
16 D. Ni, Y. Chen, H. Song, C. Liu, X. Yang and K. Cai, *J. Mater. Chem. A*, 2019, **7**, 1323–1333.
17 Y. Chen, K. Cai, C. Liu, H. Song and X. Yang, *Adv. Energy Mater.*, 2017, **7**, 1701247.
18 X. Li, C. Zhang, S. Xin, Z. Yang, Y. Li, D. Zhang and P. Yao, *ACS Appl. Mater. Interfaces*, 2016, **8**, 21373–21380.
19 H. Tang, J. Wang, H. Yin, H. Zhao, D. Wang and Z. Tang, *Adv. Mater.*, 2015, **27**, 1117–1123.
20 W. S. Hummers and R. E. Offeman, *J. Am. Chem. Soc.*, 1958, **80**, 1339.
21 Z. Xu, Z. Zhang, M. Li, H. Yin, H. Lin, J. Zhou and S. Zhuo, *J. Solid State Electrochem.*, 2019, **23**, 3419–3428.
22 U. Holzwarth and N. Gibson, *Nat. Nanotechnol.*, 2011, **6**, 534.
23 J. Shabani Shayeh, A. Ehsani, M. R. Ganjali, P. Norouzi and B. Jaleh, *Appl. Surf. Sci.*, 2015, **353**, 594–599.
24 L. J. Cote, R. Cruz-Silva and J. Huang, *J. Am. Chem. Soc.*, 2009, **131**, 11027–11032.
25 H. R. Azimi, M. Ghoranneviss, S. M. Elahi and R. Yousefi, *Ceram. Int.*, 2016, **42**, 14094–14099.
26 Q. Zhao, G. Wang, K. Yan, J. Yan and J. Wang, *J. Appl. Polym. Sci.*, 2015, **132**, 42549.
27 C. Kvarnström, H. Neugebauer, S. Blomquist, H. J. Ahonen, J. Kankare and A. Ivaska, *Electrochim. Acta*, 1999, **44**, 2739–2750.
28 C. Bora, C. Sarkar, K. J. Mohan and S. Dolui, *Electrochim. Acta*, 2015, **157**, 225–231.
29 C. Wan, Y. Jiao and J. Li, *J. Mater. Chem. A*, 2017, **5**, 3819–3831.
30 W. K. Chee, H. N. Lim, I. Harrison, K. F. Chong, Z. Zainal, C. H. Ng and N. M. Huang, *Electrochim. Acta*, 2015, **157**, 88–94.
31 Z. Xu, Z. Zhang, L. Gao, H. Lin, L. Xue, Z. Zhou, J. Zhou and S. Zhuo, *RSC Adv.*, 2018, **8**, 40252–40260.
32 L. Wang, L. Chen, B. Yan, C. Wang, F. Zhu, X. Jiang, Y. Chao and G. Yang, *J. Mater. Chem. A*, 2014, **2**, 8334–8341.
33 G. Xu, N. Wang, J. Wei, L. Lv, J. Zhang, Z. Chen and Q. Xu, *Ind. Eng. Chem. Res.*, 2012, **51**, 14390–14398.
34 H. Xu, J. Zhang, Y. Chen, H. Lu and J. Zhuang, *J. Solid State Electrochem.*, 2014, **18**, 813–819.
35 S. Mondal, U. Rana and S. Malik, *J. Phys. Chem. C*, 2017, **121**, 7573–7583.
36 L. Q. Mai, A. Minhas-Khan, X. Tian, K. M. Hercule, Y. L. Zhao, X. Lin and X. Xu, *Nat. Commun.*, 2013, **4**, 2923.
37 H.-x. Tan and X.-c. Xu, *Compos. Sci. Technol.*, 2016, **128**, 155–160.
38 V. A. Mooss and A. A. Athawale, *J. Polym. Sci., Part A: Polym. Chem.*, 2016, **54**, 3778–3786.
39 J. Zhong, S. Gao, G. Xue and B. Wang, *Macromolecules*, 2015, **48**, 1592–1597.
40 A. M. Glaudell, J. E. Cochran, S. N. Patel and M. L. Chabinyc, *Adv. Energy Mater.*, 2015, **5**, 1401072.
41 C. Yin, H. Zhou and J. Li, *Appl. Surf. Sci.*, 2019, **464**, 220–228.
42 Y.-T. Lee, M. Wang, K. Kokubo, N.-G. Kang, L. Wolf, L.-S. Tan, C.-T. Chen and L. Chiang, *Dyes Pigm.*, 2018, **149**, 377–386.
43 D. S. Patil, S. A. Pawar, J. H. Kim, P. S. Patil and J. C. Shin, *Electrochim. Acta*, 2016, **213**, 680–690.
44 D. Zhang, Y. Hao, L. Zheng, Y. Ma, H. Feng and H. Luo, *J. Mater. Chem. A*, 2013, **1**, 7584–7591.
45 A. G. Kannan, A. Samuthirapandian and D.-W. Kim, *J. Power Sources*, 2017, **337**, 65–72.
46 G.-F. Chen, X.-X. Li, L.-Y. Zhang, N. Li, T. Ma and Z.-Q. Liu, *Adv. Mater.*, 2016, **28**, 7680–7687.
47 H. Tomiyasu, H. Shikata, K. Takao, N. Asanuma, S. Taruta and Y.-Y. Park, *Sci. Rep.*, 2017, **7**, 45048.
48 W. Wang, Q. Hao, W. Lei, X. Xia and X. Wang, *J. Power Sources*, 2014, **269**, 250–259.